From Yielding to Shear Jamming in a Cohesive Frictional Suspension

Abhinendra Singh,[1,*] Sidhant Pednekar,[1,2,3,†] Jaehun Chun,[1,3,‡] Morton M. Denn,[1,2,§] and Jeffrey F. Morris[1,2,¶]
[1]Benjamin Levich Institute, CUNY City College of New York, New York, New York 10031, USA
[2]Department of Chemical Engineering, CUNY City College of New York, New York, New York 10031, USA
[3]Pacific Northwest National Laboratory, Richland, Washington 99352, USA

(Received 15 September 2018; published 7 March 2019)

Simulations are used to study the steady shear rheology of dense suspensions of frictional particles exhibiting discontinuous shear thickening and shear jamming, in which finite-range cohesive interactions result in a yield stress. We develop a constitutive model that combines yielding behavior and shear thinning at low stress with the frictional shear thickening at high stresses, in good agreement with the simulation results. This work shows that there is a distinct difference between solids below the yield stress and in the shear-jammed state, as the two occur at widely separated stress levels, with an intermediate region of stress in which the material is flowable.

DOI: 10.1103/PhysRevLett.122.098004

Introduction.—Concentrated, or *dense*, suspensions of particles in liquid are found in both natural [1] and industrial settings [2–4]. Under shear, non-Brownian suspensions display a number of non-Newtonian properties; considering just the shear properties, these mixtures may undergo yielding, shear thinning, shear thickening, or even jamming [5–8]. Such non-Newtonian rheology arises from particle interactions [7], influenced by the solid-fluid interfacial chemistry and chemical physics of both phases [9–11], as well as from frictional interactions between particles [12–14] that are influenced by roughness [15,16]. Suspensions of particles interacting by attractive forces can exhibit a yield stress and at larger stresses shear thicken, and, as discussed here, possibly jam. Shear thickening (ST), the increase of relative viscosity η_r with increasing shear rate $\dot{\gamma}$, can occur as continuous shear thickening (CST) or discontinuous shear thickening (DST) in dense suspensions; here the relative viscosity $\eta_r = \eta(\phi, \dot{\gamma})/\eta_0$ is normalized by the suspending fluid viscosity η_0, where ϕ is the particle volume fraction. The viscosity varies continuously with $\dot{\gamma}$ in CST, while DST is characterized by $\partial\eta_r/\partial\dot{\gamma} \to \infty$ at some stress, often resulting in orders of magnitude increase in viscosity. It has been demonstrated that if ϕ is sufficiently large, the suspension can even become a shear-jammed (SJ) solid [17]; this solid is fragile, in the sense that it is maintained in this state by the imposed load, and would, for example, fail if the load is applied in the reverse direction [18]. A recent body of work [19–24] has related shear thickening to a transition from lubricated to frictional interactions of particles above an "onset stress." An approach capturing this two-state model [19] based on a mean-field description of the fraction of particle interactions that are frictional has been shown [25] to be successful in describing both the relative viscosity η_r and normal stress differences found in simulations of shear thickening frictional suspensions.

To date, most study has been focused on the flow behavior of dense noncohesive suspensions. However, van der Waals forces [26], depletion forces due to dissolved noninteracting polymer [27], or the presence of an external field [9] can all lead to attractive forces between particles. A demonstrated influence of attractive forces is that the shear thickening may be obscured [9,27,28]. When the low-stress viscosity becomes sufficiently large or a yield stress develops, a suspension shear thins to a high shear-rate viscosity, which in the case of the shear-thickening suspension would be the thickened state of the noncohesive suspension [9,11,27,28].

The studies noted just above addressed volume fractions exhibiting CST. It is our particular goal to demonstrate the influence of cohesion for suspensions of volume fractions for which the noncohesive suspension undergoes DST and SJ. The latter will illustrate that the same material may exhibit shear yielding at low stress, flow at intermediate stress, and shear jamming at high stress. This provides a distinctly different picture for nearly rigid particles as to the relation of yielding and jamming than has been suggested in other work [29], as these two phenomena occur at widely separated stress levels, with an intermediate region of stresses for which the material is flowable.

We explore a broad range of volume fractions, with a focus on ϕ close to the frictional jamming volume fraction, denoted ϕ_J^μ. In this range of solid fraction, noncohesive suspensions show DST and shear jamming. We extend a constitutive model for dense frictional suspension rheology [25] to cohesive systems exhibiting yielding and shear thinning in addition to shear thickening. Using the simulation results and guided by this model, a state diagram for dense frictional suspensions with attractive interactions is proposed.

Simulations.—An assembly of inertialess spheres suspended in an equal density Newtonian fluid is simulated

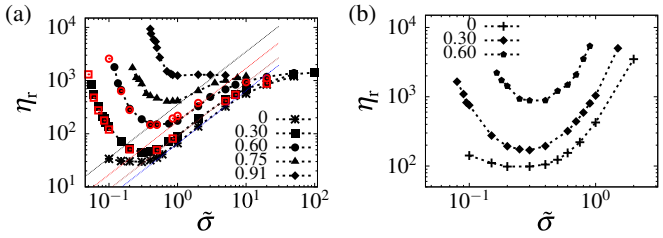

FIG. 1. Relative viscosity η_r plotted versus dimensionless applied stress $\tilde{\sigma} = \sigma/\sigma_0$ for volume fraction (a) $\phi = 0.56$ and (b) 0.6 and several values of attractive strength F_A at $\mu = 1$. The symbols are simulation data, with dashed lines provided to guide the eye. Open (red) symbols in (a) are results with 2000 particles (other cases use 500) for $F_A = 0.3$ and 0.6, showing results are very similar and finite size effects are minimal for the conditions studied here. Dotted lines in (a) show $\eta_r \propto \sigma/\sigma_0$, signifying an increase in viscosity at a constant rate, as shown in Fig. S2a [32].

under conditions of imposed shear stress σ, as described previously [30]. The suspension flows at a time-dependent shear rate $\dot{\gamma}(t)$ in a 3D Lees-Edwards periodic computational domain. We simulate 500 particles in the domain, using equal volume fractions of particles with radii a and $1.4a$. The bidispersity prevents ordering. Simulations with 2000 particles have been performed to test finite-size effects.

The particles interact through short-range hydrodynamic lubrication forces F_H, conservative forces $F_{\text{cons}} = F_A + F_R$ (where A and R denote the attractive and repulsive contributions, respectively), and contact forces F_C. The contact force allows friction, with friction coefficient μ. An electrostatic repulsion force decaying with interparticle surface separation h over a length scale defined by the Debye length λ is used: $|F_R| = F_0 \exp(-h/\lambda)$. To model the force of attraction, a van der Waals form $F_A(h) = A\bar{a}/12(h^2 + H^2)$ is used, where A denotes the Hamaker constant and $\bar{a}$ denotes the harmonic mean radius $\bar{a} = 2a_1a_2/(a_1 + a_2)$ [31]. The parameter H is fixed at $H = 0.1\bar{a}$, and is employed to eliminate the divergence of F_A at contact ($h = 0$). The conservative force is illustrated in Fig. S1 of the Supplemental Material [32]. The strength of attraction is controlled by A, which determines the value of the attractive force at contact, $F_A(0)$ (referred to as F_A in the rest of the article). The contact force between two particles is modeled by linear springs and dashpots as described elsewhere [20]. Tangential and normal components of the contact force F_C between two particles satisfy the Coulomb friction law $|F_{C,t}| \leq \mu|F_{C,n}|$, where $\mu = 1$ is used in the current work (note that $F_{C,n}$ is only compressive here.)

Simulation results.—Figure 1 shows the influence of attractive forces on the rheology of a frictional non-Brownian suspension for $\phi = 0.56$ and 0.6, where the shear stress is scaled by $\sigma_0 = F_0/6\pi a^2$ (using the smaller particle radius). To characterize the steepness of the viscosity increase in the η_r vs σ/σ_0 flow curve, the shear-thickening portion is fitted to $\eta_r \propto (\sigma/\sigma_0)^\beta$, where $\beta < 1$ signifies CST and $\beta = 1$ indicates that the shear rate, $\dot{\gamma}/\dot{\gamma}_0 = \eta_r/(\sigma/\sigma_0)$, is unchanging while stress increases and hence is the onset of DST. For $\phi = 0.56$, the noncohesive frictional suspension shows DST between two flowing states, as is evident from $\eta_r \propto \sigma/\sigma_0$ (i.e., $\beta = 1$) in Fig. 1(a). The development of a moderate yield stress σ_y is observed for $F_A = 0.3$. For $F_A \geq 0.3$, the suspension flows when $\sigma > \sigma_y$, first shear thinning from the infinite viscosity of the unyielded material and eventually shear thickening. This thickening begins continuously, but DST occurs as σ is further increased. An increase in F_A increases σ_y, which by raising the minimum viscosity reached by shear thinning effectively weakens the extent of shear thickening. For $F_A = 0$ to 0.6, discontinuous shear thickening is still observed, as shown by dotted lines indicating $\eta_r \propto \sigma/\sigma_0$. Development of a yield stress, indicated by a slope of -1 in Fig. S2a [32], does not immediately lead to obscuring of shear thickening. However, DST is not observed for $F_A = 0.75$, as only a weak shear thickening is needed to carry the suspension from its minimum viscosity to the high-stress plateau. All shear thickening is obscured with further increase in F_A, consistent with previous simulation and experimental studies at lower volume fractions [9,27,28].

At $\phi = 0.6$, exceeding the frictional jamming fraction $\phi_J^\mu \approx 0.585$ for $\mu = 1$, as shown elsewhere [25], the suspension shear jams at sufficiently large shear stress, $\sigma_{sj}(\phi)$. Upon introducing cohesion, the suspension develops a yield stress σ_y and cannot flow for $\sigma < \sigma_y$. Thus, the cohesive frictional suspension is a nonflowable solid for $\sigma < \sigma_y$, flows at intermediate stress, and shear jams above σ_{sj}. However, for $F_A = 0.91$ the suspension cannot flow for any value of shear stress, as $\sigma_y > \sigma_{sj}$. Note that below the yield stress one has a standard, albeit soft, solid that resists deformation in all directions equally if prepared without directional bias, whereas the shear-jammed solid at $\sigma > \sigma_{sj}$ is fragile in the absence of the cohesive forces, and thus has anisotropic properties [18,33].

Constitutive model.—We renormalize the scaled stress as $\hat{\sigma} = \sigma/\sigma_0^{RA}$ and shear rate as $\hat{\dot{\gamma}} = \hat{\sigma}/\eta_0$, where the scaling factor $\sigma_0^{RA} = (F_A + F_R)/6\pi a^2$ is the sum of repulsive and attractive stress at surface separation $h = 0$. In Fig. 2 we plot steady state viscosity η_r versus shear stress $\hat{\sigma}$. We observe the collapse of viscosity data for intermediate to high stress to the noncohesive flow curve. The yield stress decreases the range of stresses for which shear thickening is observed.

To quantify the effect of attractive interactions on the flow behavior of shear thickening suspensions, we use the Herschel-Bulkley equation

$$\hat{\sigma}_{\text{HB}}(\hat{\dot{\gamma}}) = \hat{\sigma}_y + K\hat{\dot{\gamma}}^n, \tag{1}$$

where $\hat{\sigma}_y$ denotes the scaled yield stress, K is the consistency index and n is the power law exponent. We find that $n = 0.5$ describes the yielding and shear-thinning behavior well for all F_A and ϕ considered here, consistent with prior studies [9,34–36]. We recast Eq. (1) as

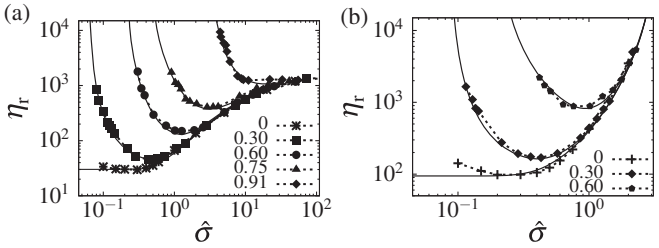

FIG. 2. Steady state flow curves for volume fractions (a) $\phi = 0.56$ and (b) 0.6 from Figs. 1(a) and 1(b) plotted versus scaled applied shear stress $\hat{\sigma} = \sigma/\sigma_0^{RA}$, $\sigma_0^{RA} = [F_A(0) + F_R(0)]/6\pi a^2$; $F_R(0)$ and $F_A(0)$ are the values of repulsive and attractive forces, respectively, at surface separation $h = 0$. The symbols are simulations with different values of strength of attraction and the solid lines are predictions from (4).

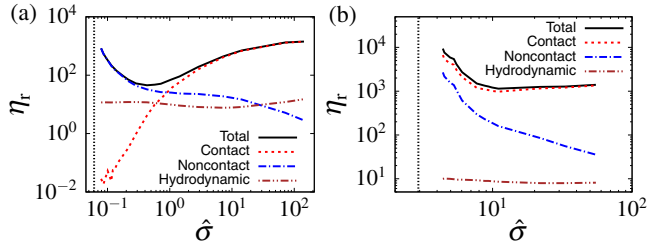

FIG. 3. Total relative viscosity (η_r) and the contributions arising from hydrodynamic interactions, conservative forces, and contact forces, plotted versus scaled shear stress $\hat{\sigma}$ for a non-Brownian suspension ($\phi = 0.56$) with (a) $F_A = 0.3$ and (b) 0.91. The broken vertical line indicates the yield stress.

$$\eta_r^{\mathrm{HB}}(\hat{\sigma}) = \frac{K^2\hat{\sigma}_y}{(\hat{\sigma} - \hat{\sigma}_y)^2} + \frac{K^2}{(\hat{\sigma} - \hat{\sigma}_y)}. \tag{2}$$

The model parameters $\hat{\sigma}_y$ and K are obtained by fitting the low stress (yielding and shear thinning) portion of the flow curve to Eq. (2). The shear thickening of the noncohesive suspension viscosity has been expressed as [25]

$$\eta_r^C(\phi, \hat{\sigma}) = \alpha_m(\hat{\sigma})[\phi_m(\hat{\sigma}) - \phi]^{-2}, \tag{3a}$$

where

$$\phi_m(\hat{\sigma}) = \phi_J^{\mu} f(\hat{\sigma}) + \phi_J^0[1 - f(\hat{\sigma})] \tag{3b}$$

and

$$\alpha_m(\hat{\sigma}) = \alpha^{\mu} f(\hat{\sigma}) + \alpha^0[1 - f(\hat{\sigma})] \tag{3c}$$

interpolate between two values of ϕ and α, while $f \in [0, 1]$ represents the fraction of frictional contacts, whose form is presented in Mari *et al.* [20]. As in earlier works [9,27,35], various contributions to the viscosity can be superimposed as

$$\eta_r(\phi, \hat{\sigma}) = \eta_r^{\mathrm{HB}}(\phi, \hat{\sigma}) + \eta_r^C(\phi, \hat{\sigma}). \tag{4}$$

The viscosity modeled by Eq. (4) is compared to the simulation data in Fig. 2 and is seen to agree well. We also find that the second normal stress difference N_2 (shown in Supplemental Material [32], Fig. S8) behaves in a fashion similar to the shear stress; i.e., it displays cohesion-dependent yield behavior at low stress while the behavior is independent of attraction at high stress. In Fig. S7 [32], we demonstrate a possible extension of the model to noncohesive Brownian suspensions capturing well both Brownian shear thinning and frictional shear thickening.

Origin of yielding.—In an attempt to get a more mechanistic understanding of the behavior of cohesive shear-thickening systems, we focus on the origin of yielding, especially with increasing force of attraction. Subsequently, we separate the total viscosity into contact and noncontact contributions, which are shown as functions of stress $\hat{\sigma}$ for $F_A = 0.3$ and 0.91 in Figs. 3(a) and 3(b), respectively. The hydrodynamic contribution to overall viscosity is insignificant for the conditions presented. At low strengths of attraction, noncontact (attractive and repulsive) forces provide the dominant contribution to overall viscosity at low stresses, while the contact contribution takes over at higher stresses. Snapshots of force networks for $F_A = 0.3$ at low stress are presented in Fig. S4a [32]. Particles are seen to interact only via finite-range (noncontact) forces. On closer inspection, repulsive forces are seen to interact primarily along the compressive axis as they resist approaching particles. Attractive forces, by contrast, generate resistance along the extensional axis for departing particles.

In stark contrast, for high strength of attraction the dominant contribution is from contact forces, because the potential minimum is comparable to the lubrication cutoff length, bringing particles into contact, irrespective of applied stress [as seen in Fig. 3(b)]. This can be confirmed by the presence of frictional force networks in the system even at low stress (Fig. S4b [32]). Figure 2(a) provides insight into this behavior; the yield stress for $F_A = 0.91$ is larger than the onset stress $\hat{\sigma}_{\mathrm{on}} \doteq 0.3$ for the noncohesive ($F_A = 0$) curve. While the cause of the yield stress is found in the strong attractive forces, these forces bring particles into contact to allow formation of the frictional force networks seen in Fig. S4b [32]. Frictional contacts are capable of resisting an applied shear stress, leading to an increase in yield stress and viscosity.

Flow-state diagram.—Using the simulation results of the present work (see data in Fig. S9 [32]), we construct a flow-state diagram in the $\hat{\sigma}$-ϕ plane, as shown in Fig. 4 for $F_A = 0.3$. Since the focus of the present study is on the rheological behavior for volume fractions close to DST or above, we have only probed volume fractions $\phi \geq 0.52$. For the range of volume fraction $\phi_J^{\mu} < \phi < \phi_y^m$ the suspension is in different solid states for $\hat{\sigma} < \hat{\sigma}_y$ and $\hat{\sigma} > \hat{\sigma}_{sj}$. There is a volume fraction ϕ_y^m above which flow does not occur at any stress $\hat{\sigma}$. With increasing ϕ the range of stress $\hat{\sigma}$ for which the system can flow shrinks until it vanishes at ϕ_y^m. For $\phi < \phi_J^{\mu}$ the system is in an unyielded solid state for $\sigma < \sigma_y$, with flow at larger stresses. The yield stress increases with ϕ

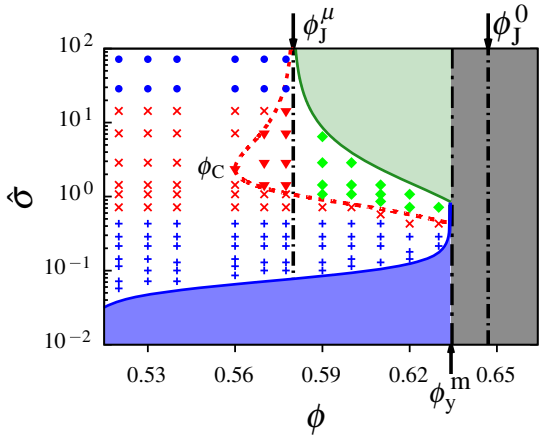

FIG. 4. Flow-state diagram in the $\hat{\sigma}$-ϕ plane for $F_A = 0.3$ showing shear jammed (green), unyielded (blue), flowing (white), and inaccessible (gray) states. The green and blue solid lines are the stress-dependent jamming and yield lines, respectively, while the red dashed line is the DST line and shows the locus of points where $\partial\dot{\gamma}/\partial\sigma = 0$. Dot-dashed black lines show ϕ_J^μ, ϕ_y^m, and ϕ_J^0. Symbols show different flowing states of the suspension: Shear thinning (blue plusses), shear thickened state (blue circles), CST (red crosses), DST between two flowing states (red inverted triangles), DST between a flowing and a jammed state (green diamonds). Here, we have only probed volume fractions $\phi \geq 0.52$, and the yield line might continue for lower volume fractions.

and diverges at ϕ_y^m, which is smaller than ϕ_J^0; this behavior has also been observed previously for other non-Brownian suspensions [37]. For volume fractions below ϕ_C, CST is observed for intermediate stress values. For $\phi_C \leq \phi < \phi_J^\mu$, DST is observed between two flowing states, as shown by the dashed (red) line, which is the locus of points where $\partial\dot{\gamma}/\partial\sigma = 0$, while for $\phi_J^\mu < \phi < \phi_y^m$ the upper boundary of DST states is the stress-dependent jamming line $\phi_m(\hat{\sigma})$ shown by the solid (green) line. A similar flow-state diagram was proposed recently [38] using constraint counting arguments. Since we present the state diagram for a single nonzero F_A, we note that at $F_A = 0$ the state diagram would reduce to the one proposed previously [25]. It is beyond the scope of this study, but we note that higher values of F_A at $\phi > \phi_J^\mu$ could result in a completely unflowable material; i.e., the attractive forces would pull the system into a contact network from which it could not yield, although an applied stress might cause deformation of contacts that would relax upon removal of stress.

Equations (2) and (4) demonstrate how the development of yield stress and shear thinning shrinks the range of stress for which shear thickening is observed. For a given volume fraction ϕ, increasing F_A leads to an increase in yield stress $\hat{\sigma}_y$, which in turn increases both $\hat{\sigma}_{\text{on}}$ and the viscosity at the onset of shear thickening. The viscosity at $\hat{\sigma}_{\text{on}}$ should follow $\eta_r(\hat{\sigma}_{\text{on}}, \phi) \leq \eta_r^\mu(\phi)$, where $\eta_r^\mu(\phi)$ is the viscosity of the thickened (frictional) state. At the equality shear thickening is obscured, implying that the system yields and shear thins directly to the frictional branch.

Conclusions.—In this work we have studied the rheology of dense suspensions interacting through both finite-range cohesive and frictional contact interactions. We report flow curves that show yielding behavior at low stress and shear thickening as well as jamming at high stress, depending on the volume fraction ϕ relative to its frictional jamming value ϕ_J^μ. This yield to jamming within a single concentration suspension has been conceptualized [39], but never previously reported from experiment or simulation. This behavior provides a clear distinction between yielding and jamming for nearly rigid particles, unlike other suggestions that these phenomena are essentially the same [29]. The distinction becomes complicated when the particles have a finite elastic modulus (e.g., yielding at stresses above jamming may take place [40]). It is important to note that the yielding behavior we consider is due to attractive forces; a finite-range repulsive force could lead to a glasslike yielding behavior but this is not considered.

We have proposed a constitutive model that captures the observed behavior. The yield stress $\hat{\sigma}_y$ depends on the strength of attraction, which in principle can be controlled by particle size, microstructure, chemistry at solid-fluid interfaces, and properties of fluid and solid phases, such as dielectric properties [9,11,34,41,42].

Our work thus provides fundamental insight into the complex rheological behavior of particle suspensions based on balances between shearing, conservative, and frictional forces. Although we have used specific force profiles for the repulsive and attractive forces, modeling electrostatic repulsion and van der Waals attraction, respectively, the modeling of rheology of dense suspensions, and the proposed state diagram, should be qualitatively similar for generic attractive and repulsive forces. Additionally, the proposed state diagram can, in principle, be extended to encompass systems that exhibit shear thinning because of Brownian effects.

We thank Ryohei Seto for useful discussions. The computation in this work was supported, in part, under National Science Foundation Grants No. CNS-0958379, No. CNS-0855217, No. ACI-1126113, and the City University of New York High Performance Computing Center at the College of Staten Island. J. F. M. was supported by NSF 1605283. Discussion on particle forces (J. C.) was supported by the Interfacial Dynamics in Radioactive Environments and Materials (IDREAM), an Energy Frontier Research Center funded by the U.S. Department of Energy (DOE), Office of Science, Basic Energy Sciences.

*asingh.iitkgp@gmail.com
†sidhant11@gmail.com
‡jaehun.chun@pnnl.gov
§denn@ccny.cuny.edu
¶morris@ccny.cuny.edu

[1] P. Coussot, *Mudflow Rheology and Dynamics* (Balkema Publishers, Rotterdam, 1997).
[2] J. Benbow and J. Bridgewater, *Paste Flow and Extrusion* (Oxford University Press, Oxford, 1993).
[3] J. Chun, T. Oh, M. Luna, and M. Schweiger, Colloids Surf. A **384**, 304 (2011).
[4] R. A. Peterson, E. C. Buck, J. Chun, R. C. Daniel, D. L. Herting, E. S. Ilton, G. J. Lumetta, and S. B. Clark, Environ. Sci. Technol. **52**, 381 (2018).
[5] J. Mewis and N. J. Wagner, *Colloidal Suspension Rheology* (Cambridge University Press, Cambridge, England, 2011).
[6] E. Guazzelli and J. F. Morris, *A Physical Introduction to Suspension Dynamics* (Cambridge University Press, Cambridge, England, 2011).
[7] M. M. Denn and J. F. Morris, Annu. Rev. Chem. Biomol. Eng. **5**, 203 (2014).
[8] M. M. Denn, J. F. Morris, and D. Bonn, Soft Matter **14**, 170 (2018).
[9] E. Brown, N. A. Forman, C. S. Orellana, Z. Hanjun, B. W. Maynor, D. E. Betts, J. M. DeSimone, and H. M. Jaeger, Nat. Mater. **9**, 220 (2010).
[10] E. Brown and H. M. Jaeger, Rep. Prog. Phys. **77**, 046602 (2014).
[11] L. Oyarte Gálvez, S. de Beer, D. van der Meer, and A. Pons, Phys. Rev. E **95**, 030602 (2017).
[12] J. Comtet, G. Chatté, A. Niguès, L. Bocquet, A. Siria, and A. Colin, Nat. Commun. **8**, 15633 (2017).
[13] N. Fernandez, R. Mani, D. Rinaldi, D. Kadau, M. Mosquet, H. Lombois-Burger, J. Cayer-Barrioz, H. J. Herrmann, N. D. Spencer, and L. Isa, Phys. Rev. Lett. **111**, 108301 (2013).
[14] C.-P. Hsu, S. N. Ramakrishna, M. Zanini, N. D. Spencer, and L. Isa, Proc. Natl. Acad. Sci. U.S.A. **115**, 5117 (2018).
[15] D. Lootens, H. van Damme, Y. Hémar, and P. Hébraud, Phys. Rev. Lett. **95**, 268302 (2005).
[16] L. C. Hsiao, S. Jamali, E. Glynos, P. F. Green, R. G. Larson, and M. J. Solomon, Phys. Rev. Lett. **119**, 158001 (2017).
[17] I. R. Peters, S. Majumdar, and H. M. Jaeger, Nature (London) **532**, 214 (2016).
[18] M. E. Cates, J. P. Wittmer, J.-P. Bouchaud, and P. Claudin, Phys. Rev. Lett. **81**, 1841 (1998).
[19] M. Wyart and M. E. Cates, Phys. Rev. Lett. **112**, 098302 (2014).
[20] R. Mari, R. Seto, J. F. Morris, and M. M. Denn, J. Rheol. **58**, 1693 (2014).
[21] R. Seto, R. Mari, J. F. Morris, and M. M. Denn, Phys. Rev. Lett. **111**, 218301 (2013).
[22] N. Y. C. Lin, B. M. Guy, M. Hermes, C. Ness, J. Sun, W. C. K. Poon, and I. Cohen, Phys. Rev. Lett. **115**, 228304 (2015).
[23] B. M. Guy, M. Hermes, and W. C. K. Poon, Phys. Rev. Lett. **115**, 088304 (2015).
[24] R. Mari, R. Seto, J. F. Morris, and M. M. Denn, Proc. Natl. Acad. Sci. U.S.A. **112**, 15326 (2015).
[25] A. Singh, R. Mari, M. M. Denn, and J. F. Morris, J. Rheol. **62**, 457 (2018).
[26] B. J. Maranzano and N. J. Wagner, J. Rheol. **45**, 1205 (2001).
[27] V. Gopalakrishnan and C. Zukoski, J. Rheol. **48**, 1321 (2004).
[28] S. Pednekar, J. Chun, and J. F. Morris, Soft Matter **13**, 1773 (2017).
[29] A. J. Liu and S. R. Nagel, Annu. Rev. Condens. Matter Phys. **1**, 347 (2010).
[30] R. Mari, R. Seto, J. F. Morris, and M. M. Denn, Phys. Rev. E **91**, 052302 (2015).
[31] W. B. Russel, D. A. Saville, and W. R. Schowalter, *Colloidal Dispersions* (Cambridge University Press, Cambridge, England, 1992).
[32] See Supplemental Material at http://link.aps.org/supplemental/10.1103/PhysRevLett.122.098004 for details.
[33] D. Bi, J. Zhang, B. Chakraborty, and R. P. Behringer, Nature (London) **480**, 355 (2011).
[34] B. J. Maranzano and N. J. Wagner, J. Chem. Phys. **114**, 10514 (2001).
[35] A. Zaccone, D. Gentili, H. Wu, M. Morbidelli, and E. Del Gado, Phys. Rev. Lett. **106**, 138301 (2011).
[36] S. Dagois-Bohy, S. Hormozi, É. Guazzelli, and O. Pouliquen, J. Fluid Mech. **776**, R2 (2015).
[37] J. Z. Zhou, P. H. Uhlherr, and F. T. Luo, Rheol. Acta **34**, 544 (1995).
[38] B. M. Guy, J. A. Richards, D. J. M. Hodgson, E. Blanco, and W. C. K. Poon, Phys. Rev. Lett. **121**, 128001 (2018).
[39] N. J. Wagner and J. F. Brady, Phys. Today **62**, 10, 27 (2009).
[40] K. N. Nordstrom, E. Verneuil, P. E. Arratia, A. Basu, Z. Zhang, A. G. Yodh, J. P. Gollub, and D. J. Durian, Phys. Rev. Lett. **105**, 175701 (2010).
[41] P. J. Scales, S. B. Johnson, T. W. Healy, and P. C. Kapur, AIChE J. **44**, 538 (1998).
[42] Z. Zhou, P. J. Scales, and D. V. Boger, Chem. Eng. Sci. **56**, 2901 (2001).